Representing the Indian Ocean Dipole

M. R. Jury [1, 2] ✉

[1] *University of Zululand, KwaDlangezwa, South Africa*
[2] *University of Puerto Rico Mayaguez, Puerto Rico, USA*
✉ *mark.jury@upr.edu*

Abstract

Purpose. This paper offers an alternative representation of the Indian Ocean Dipole. Instead of the zonal gradient of equatorial sea surface temperature, the new index uses tropical sub-surface temperatures (T100).

Methods and Results. The space-time character of the new index is defined by empirical orthogonal function analysis in the domain 20°S–5°N, 35°–120°E. The spatial pattern reflects an inherent zonal dipole with a temporal score that correlates with atmospheric empirical orthogonal function modes that describe the Walker circulation and basin-scale convection. Statistical regressions are conducted in the period 1979–2019 to evaluate the traditional Dipole Mode Index and the new T100 index, and the association with East Africa climate and Pacific Nino3.4 SST. These demonstrate improved performance of the T100 index with ~ 30% higher r^2 explained variance.

Conclusions. Whereas the old index tracks feedback between equatorial sea surface temperature / zonal wind / surface fluxes, the new index tracks coupling between south Indian Ocean Rossby waves / anticyclonic curl / thermocline oscillations.

Keywords: Indian Ocean, dipole, subsurface representation, tropical sub-surface temperatures, anticyclonic curl, thermocline oscillations

Introduction

Zonal oscillations of the Indian Ocean Dipole (IOD) are coupled with the regional atmospheric circulation and global El Niño Southern Oscillation (ENSO) [1– 13]. As El Niño commences, easterly winds spread into the equatorial east Indian Ocean. The anticyclonic wind stress curl induces downwelling ocean Rossby waves that propagate westward across the south Indian Ocean. These have a resonant period of ±4 years and amplify along the thermocline ridge (Seychelles dome 5°–15°S) [14–19]. Sinking motions and warmer sea surface temperatures (SST) in the west Indian Ocean trigger atmospheric convection and diabatic heating [20–24], a feature evident in multi-model ensembles [8, 25, 26]. The mature phase of IOD in boreal autumn is preceded by Rossby-Kelvin wave transformation and reflection from the basin edges [27].

This paper offers an alternative index for the IOD and evaluates how it represents interannual climate variability around the basin by statistical analysis. Our focus is on index formulation and performance of equatorial surface feedback versus off-equatorial sub-surface coupling [28–31]. This work is motivated by widespread use

of the SST-based Dipole Mode Index (DMI) [4] to track the IOD: <psl.noaa.gov/gcos_wgsp/Timeseries/DMI/>, <www.bom.gov.au/climate/iod/>, <stateoftheocean.osmc.noaa.gov/sur/ind/>, <climexp.knmi.nl/selectindex.cgi?> …monthly climate indices, <iridl.ldeo.columbia.edu/SOURCES/.NOAA/.NCDC/.ERSST/.version4/.IOD/>, <climate.copernicus.eu/charts/c3s_seasonal/ …then SST plumes: area=iod> (where … refers to the need for browser search). The main scientific question is whether an off-equatorial sub-surface index better reflects the Indian Ocean Dipole?

Data and methods

We represent the IOD via monthly 1–100 m depth-averaged sea temperatures (T100) assimilated by the National Ocean Data Center (NODC) [32]; and by sea surface height (SSH) derived from ocean reanalyses such as the Global Ocean Data Assimilation System (GODAS) [33]; Simple Ocean Data Assimilation (SODA3) [34]; European Community satellite Altimeter (EC-ALT) [35]. The SSH is synonymous with dynamic topography, while depth averaged sea temperatures characterize ocean heat content. These reanalysis products (T100, SSH) have a minimum horizontal resolution of 50 km, which reflects the east-west dipole. Monthly atmospheric reanalysis 'surface' (10 m) and upper-level zonal winds and vertical motion from the European Community (ERA5) [36] and NOAA satellite net Outgoing Long-wave Radiation data (OLR) [37] quantify the wind circulation and atmospheric convection over the Indian Ocean. Climate responses over East Africa (eafr) 8°S–9°N, 28°–46°E emerge from Climate Hazards InfraRed Precipitation with Stations (CHIRPS2) [38] and satellite vegetation color (NDVI) [39].

All monthly time series (1979–2019) including the DMI, are standardized, detrended, and polynomial filtered [40] to retain periods above 1.5 years [19]. The filters eliminate intra-seasonal noise and long-term warming trends. Empirical orthogonal functions (EOF) are calculated on fields of T100, SSH, OLR, and zonal winds over the domain 20°S–5°N, 35°–120°E. This domain captures the off-equatorial ocean Rossby wave that undulates on the thermocline ridge ~ 8°S [16, 24, 41, 42]. Many readers will be familiar with the EOF calculation which generates a spatial loading pattern and associated temporal score for each distinct mode. For most parameters the first mode accounts for about one-third of total variance (range 26–40%). The T100, SSH, OLR EOF1 loadings form two opposing centers of action reflecting zonal dipoles in +IOD phase, while surface and 200 hPa zonal wind EOF1 cluster over the central basin. Previous work [43] applied EOF analysis to depth-of-20C-isotherm in the tropical Indian Ocean, consistent with our study. EOF analyses were repeated using a variety of ocean reanalyses and confirmed that the T100 spatial pattern and temporal score presented here is both stable and inter-changeable.

Filtered temporal scores are analyzed for wavelet spectra [44], and for correlation with the traditional DMI formulated as SST west 10°S–10°N, 50°–70°E minus SST east 10°S–0°N, 90°–110°E, the Pacific Nino3.4 SST (5°S–5°N, 170°–120°W), and East Africa (eafr) rainfall and vegetation (8°S–9°N, 28°–46°E). Pearson-product correlations are computed for lags – 6 to + 6 months. The degrees-of-freedom is estimated as the record length divided by filter = 468/18 months [45], hence statistical significance above 99% confidence requires $|r| > 0.48$ or r^2 variance > 0.23.
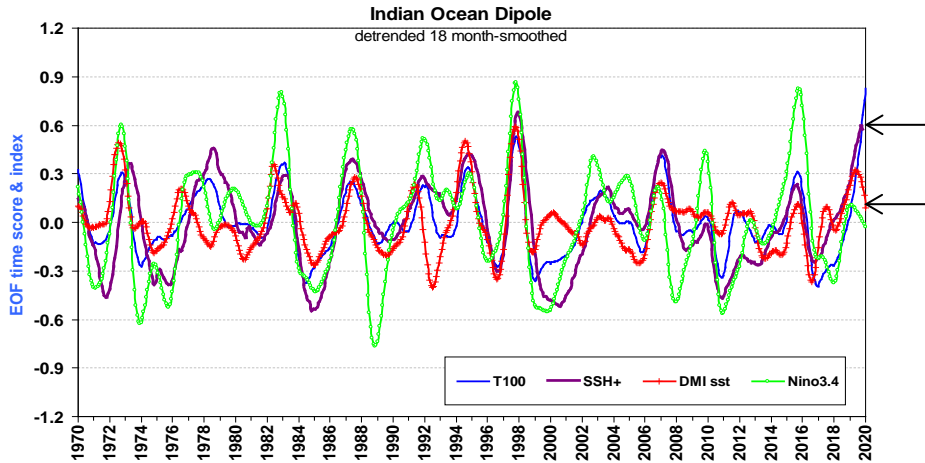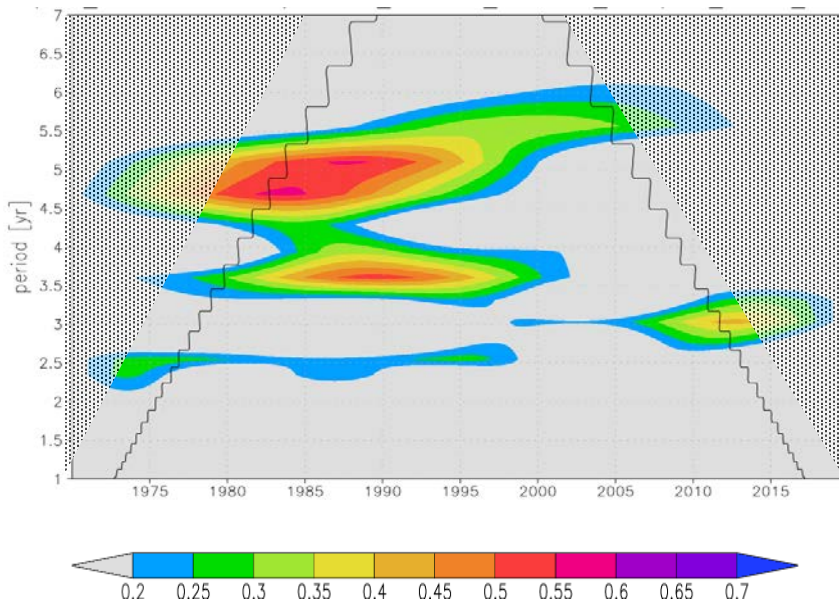
F i g. 1. EOF1 temporal scores and SST indices, all 1.5-year filtered and detrended, similar to Fig. 3, *d*. The 2019 event (arrows) is captured by T100 and SSH indices, while the DMI turns downward with Nino3.4 (*a*); wavelet spectral analysis of filtered Nino3.4 SST, for comparison with Fig. 3, *e* (*b*)

The evolving nature of IOD teleconnections is studied by five-year running regressions which cover the spectral energy in wavelet analysis. The sample 'window' requires a standardized value > |0.72| for 90% confidence (note: outcomes were similar for 3–7-year windows). Large amplitude +IOD events (based on T100) are analyzed as composites: October – December 1982, 1994, 1997, 2006, 2015 in zonal sections of atmosphere and ocean anomalies, and as hovmoller plots of SSH anomalies from 1 year before to 1 year after the event.

Atmospheric composites are equatorial averaged (5ºN–5ºS) while the oceanic composites cover the thermocline ridge (5º–15ºS), thus accounting for anticyclonic curl that generates the off-equatorial Rossby wave. The mean annual cycle of +IOD events is calculated to demonstrate seasonal amplification in boreal autumn. Naturally, these tend to be preceded and followed by –IOD events (Fig. 1).

We compare statistical outcomes for the surface DMI and sub-surface T100 (Table 1), not to debate the physical processes nor to relegate the DMI, but to identify benefits of the new index.

T a b l e 1

Cross-correlation of temporal series

	DMI sst	Nino3.4	T100	SSH	−Usfc	U200	OLR	eafr rain
Nino3.4	0.40							
T100	**0.59**	**0.73**						
SSH	0.45	**0.63**	**0.80**					
−Usfc	**0.67**	**0.75**	**0.88**	**0.75**				
U200	0.39	**0.78**	**0.65**	**0.55**	**0.70**			
OLR	**0.65**	**0.63**	**0.83**	**0.61**	**0.92**	**0.56**		
eafr rain	0.27	0.33	0.45	0.40	0.44	0.35	0.46	
eafr NDVI	0.05	0.45	**0.51**	**0.51**	0.40	0.33	0.42	0.19

N o t e: Cross-correlation of temporal series: DMI & Nino3.4 indices; T100, SSH, OLR are EOF1 dipole scores (cf. Fig. 3, *d*) with warm / west +IOD (cf. Fig. 3, *a – c*); EOF1 zonal winds in central basin are –surface (reversed) & + aloft (200 hPa) as indicated by arrows in Fig. 3, *b, c*. East Africa (eafr) rain and NDVI time series are +wet (cf. Fig. 7, *c*). Degrees of freedom equal 468 / 18 in the period 1980–2018, with r > 0.48 significant at 99% confidence (bold).

EOF analysis ensures a steady representation of the IOD across improving technology (altimetry, profiling floats) and provides a sensible and objective way to cluster dipole features that tend to magnify in October – December season at two centers of action. The new index encompasses sub-surface / off-equatorial / low-frequency signals that modulate the IOD and dictate what data / domain / filter should be used. Online resources such as the KNMI Climate Explorer, are available to obtain the new index for universal application. Global ocean data assimilation blends satellite and *in situ* measurements (Fig. 2) for real-time input to coupled model projections of ocean heat content (T100, SSH), which characterize the IOD.
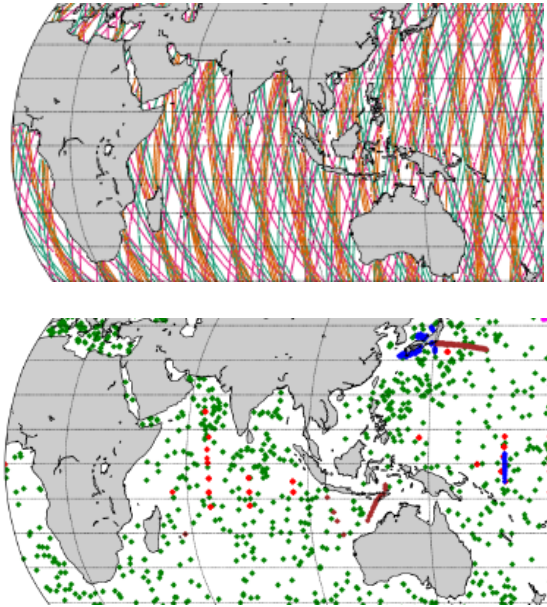
F i g. 2. Example of operational technology which characterizes ocean heat content (T100, SSH): satellite altimeter tracks over a 5-day period in 2019 (*top*); dots of profiling floats and buoys reporting temperature (*bottom*)

Results

We first consider the location of DMI 'nodes' relative to the spatial loading patterns of EOF1 T100, SSH and OLR (Fig. 3, *a – c*). The eastern DMI node is well positioned however the western DMI node is symmetrical about the equator and less focused on the southern thermocline ridge. Evaluating the temporal score, we note that interannual filtering removes only 16–18% of raw T100 or SSH r^2 explained variance compared with the noisy DMI at 51%. The SSH EOF1 scores are better correlated with filtered T100 (r = 0.80) than the DMI (r = 0.45; Table 1). Summing the pair-wise correlations in Table 1 yields the DMI = 3.47 compared with T100 = 5.44. Wavelet spectral analysis of the filtered T100 temporal score (Fig. 3, *d, e*) reflects 3–5-year cycling; whereas Nino3.4 (cf. Fig. 1, *b*) has more spectral energy at 5–6-year consistent with slower resonance in the Pacific [46].

Composite analysis of five large amplitude +IOD events (Fig. 4, *a – c*) illustrates the zonal overturning (equatorial Walker) atmospheric circulation: deep easterly flow over the central Indian Ocean, moist rising motions in the west and dry sinking motions in the east, and upper-level westerly flow above 7 km. Similarly, the oceanic section at +IOD reflects a thermal dipole in the 40–120 m layer connected by westward surface currents and rising / sinking motions at 95°E / 55°E. The hovmoller plot of composite SSH illustrates the diagonal crest associated with a transient ocean Rossby wave moving westward along ~ 8°S at 0.14 m/s consistent with [16]. Its coupling with the overlying atmospheric circulation and convection is responsible for the coherent rhythm in EOF1 temporal scores (cf. Fig. 3, *d*). Mean annual cycle amplitude increases in October – December season, as indicated by EOF1 upper quintiles in Fig. 4, *d*. Thus, our new index retains seasonal phase-locking.
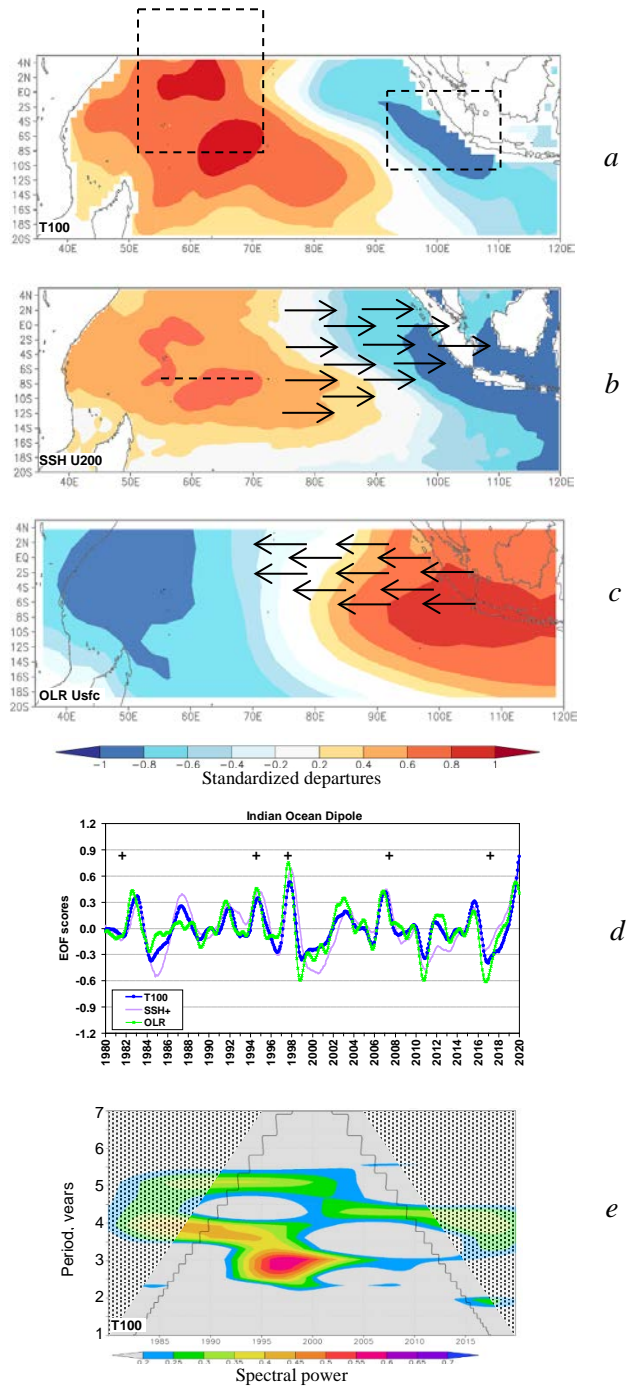
F i g. 3. EOF1 standardized spatial loading patterns for: *a* – T100 (dashed boxes refer to DMI); *b* – SSH with schematic arrows representing upper wind EOF1 '+U200'; *c* – OLR with schematic arrows representing surface wind EOF1 '−Usfc'; vectors below 1 σ omitted; *d* – EOF1 filtered temporal scores; *e* – T100 wavelet spectral energy shaded above 98% confidence with cone of validity. Dashed line in *b* refers to the Seychelles dome; plus symbols in *d* are composite IOD events in Fig. 4. Note that the western DMI node extends beyond our EOF1 domain in *a*
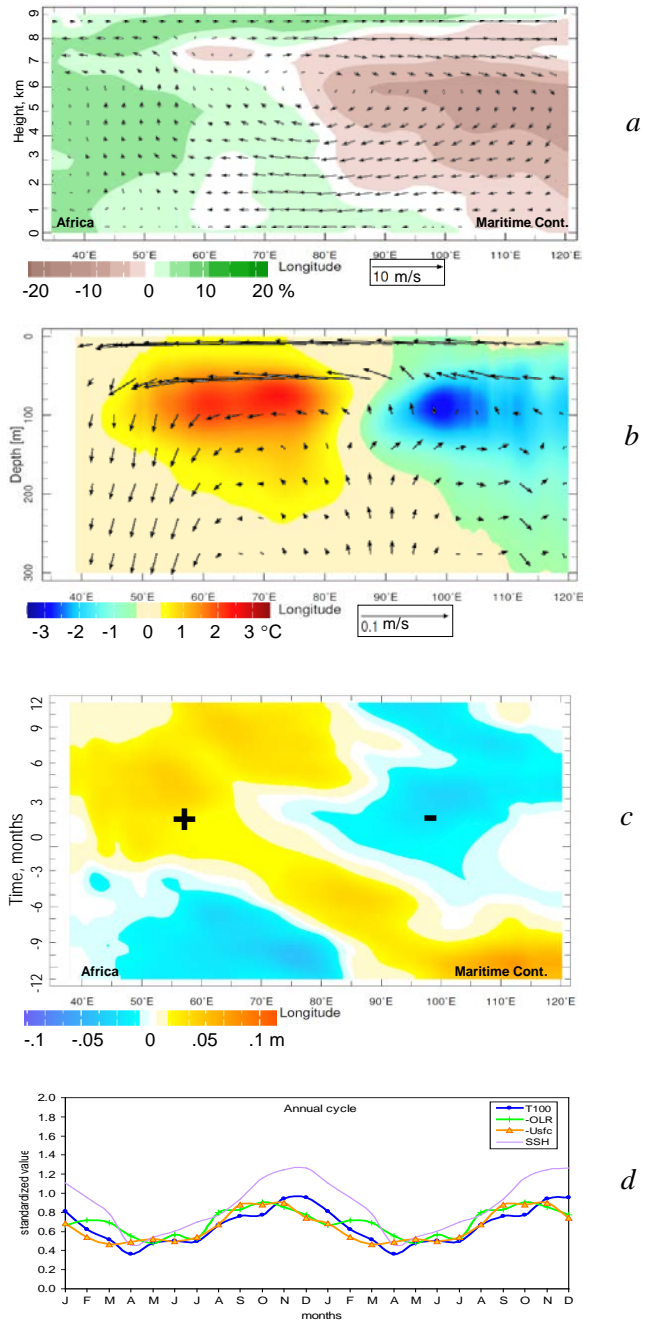
F i g. 4. Composite +IOD events October – December 1982, 1994, 1997, 2006, 2015: *a* – atmospheric section averaged 5°N–5°S of zonal winds & vertical motion (vectors) and relative humidity anomalies (shaded); *b* – ocean section averaged 5°–15°S of zonal currents & vertical motion (vectors) and temperature anomalies (shaded); *c* – composite hovmoller plot of SSH anomalies averaged 5°–15°S from –12 to +12 months for the same +IOD events, with centers of action +/–; and insignificant results shaded neutral; *d* – annual cycle x2 of EOF1 scores for the upper quintile of +IOD events; e.g. duplicated to reflect austral summer. Note that in (*a* – *c*) neutral shading is insignificant, in (*a, b*) vertical motion is converted to join the zonal flow and exaggerated
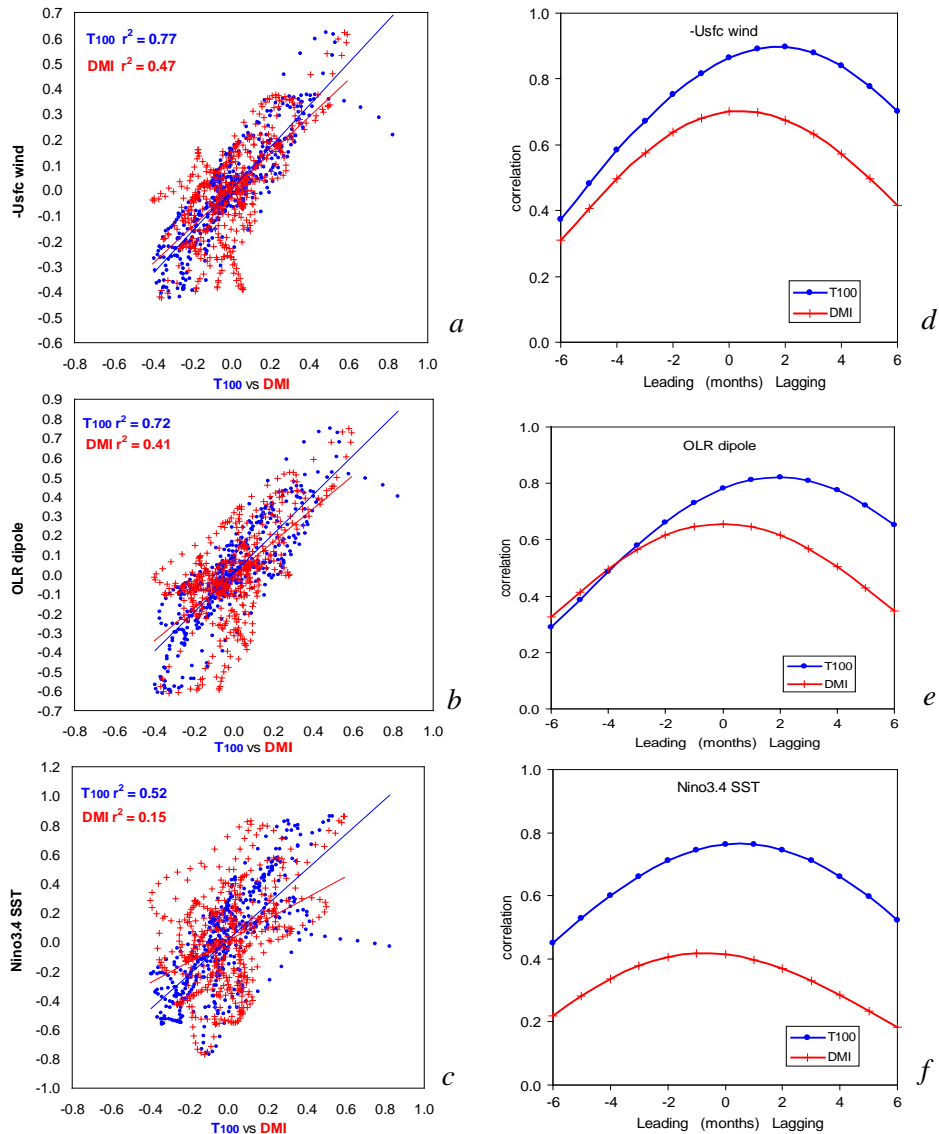
F i g. 5. *On the left* – scatterplots of filtered T100 EOF1 and DMI time series compared (at 0 lag) with: *a* – EOF1 −Usfc wind; *b* – EOF1 OLR; and *c* – Nino3.4 SST with regression fit listed. *On the right* – lag correlations of filtered T100 EOF1 and DMI time series versus: *d* – EOF1 −Usfc wind; *e* – EOF1 OLR; and *f* – Nino3.4 SST. Correlations with other variables are listed in Table 1. Positive values refer to +IOD phase (warm & moist / west)

Side-by-side comparisons of the filtered DMI and T100 with the Indian Ocean surface wind (−Usfc, eg. easterly positive) and OLR dipole EOF1 temporal scores, and the Pacific Nino3.4 SST are presented as scatterplots (Fig. 5, *a – c*) and lag-correlations (Fig. 5, *d – f*). The scatterplot regressions indicate that T100 achieves ~ 30% higher r^2 explained variance than the DMI. We infer the upper ocean is well coupled to local wind and convection, but negative events (lower left of scatterplots) tend to drift away from the regression line. Temporal lag correlations demonstrate the DMI begins (− 6 months before) with similar influence but

gradually falls behind T100 by + 2 months after. Hence the T100 better couples with Walker Cell modulated convection (−Usfc, OLR dipole), consistent with the simulations of [47]. The DMI is less sensitive to Pacific modulation (represented by filtered Nino3.4); its r value remains < 0.4 across all lags.

The evolution of IOD teleconnections is illustrated in Fig. 6, *a, b* via five-year running regressions. The T100 reflects steady coupling: standardized values are ~ 1 with respect to Indian OLR and −Usfc wind, and dip in 1987–1990 and 2004–2009 with respect to Nino3.4. On the other hand, five-year running regressions with DMI are unstable. Standardized values are ~ 1 in 1980–1996 and 2003–2006 with the Indian variables but decline in the 2000 and 2011 events. The DMI decouples from Nino3.4 much of the time and only nears unity from 1992–1997. The research [48] shows that the IOD is both internally and externally triggered, so indices should account for either pathway – as the T100 does.

a

b
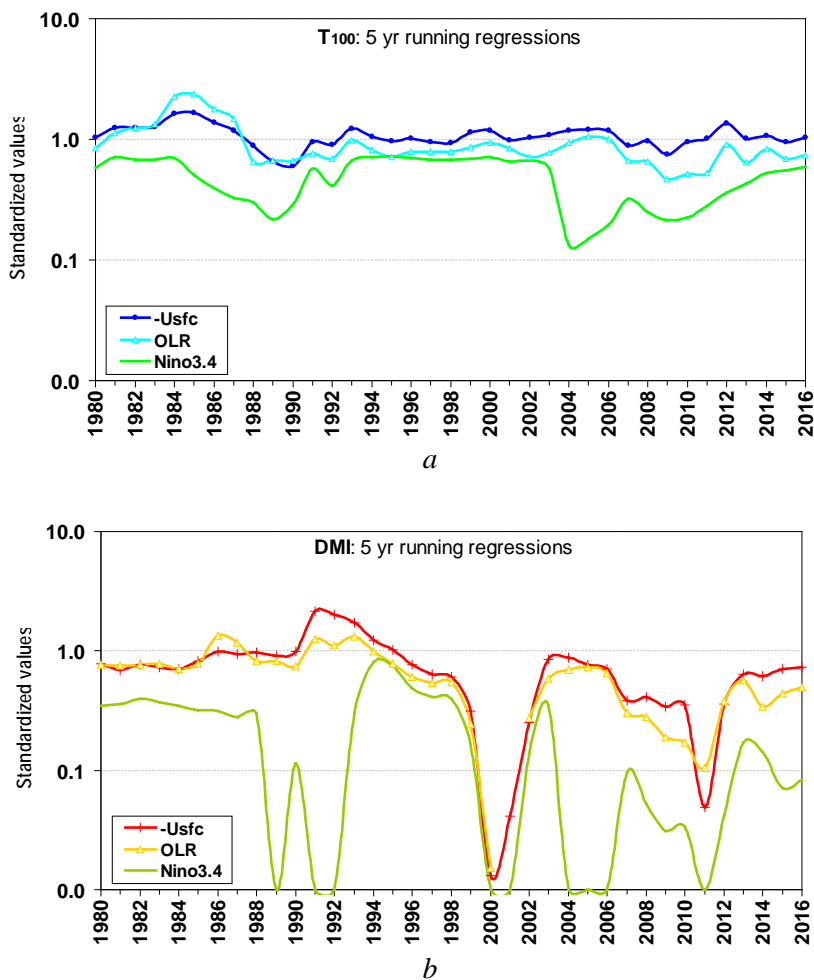
F i g. 6. Five-year running regressions between the filtered standardized temporal scores of −Usfc wind, OLR, and Nino3.4 SST: *a* – T100 EOF1; *b* – DMI. The end of record is truncated by the 5-year window; standardized values are plotted in log-scale, with 90% confidence > 0.72

One of the regions affected by the IOD is East Africa [49, 50], where rainfall

and vegetation drive agricultural consequences. Lag correlations with rainfall demonstrate that T100 offers good performance at 2–4 month lead time than DMI and Nino3.4 indices (Fig. 7, *a*). There is more distinction for NDVI, wherein the T100 covers 31% of r^2 explained variance compared with the DMI at only 1% r^2 (Fig. 7, *b*). Previous research has revealed IOD modulation of East Africa rainfall in September – December season [49] but results here suggest a wider temporal influence by the T100 dipole. A more reliable index for the Indian Ocean Dipole could pay dividends.
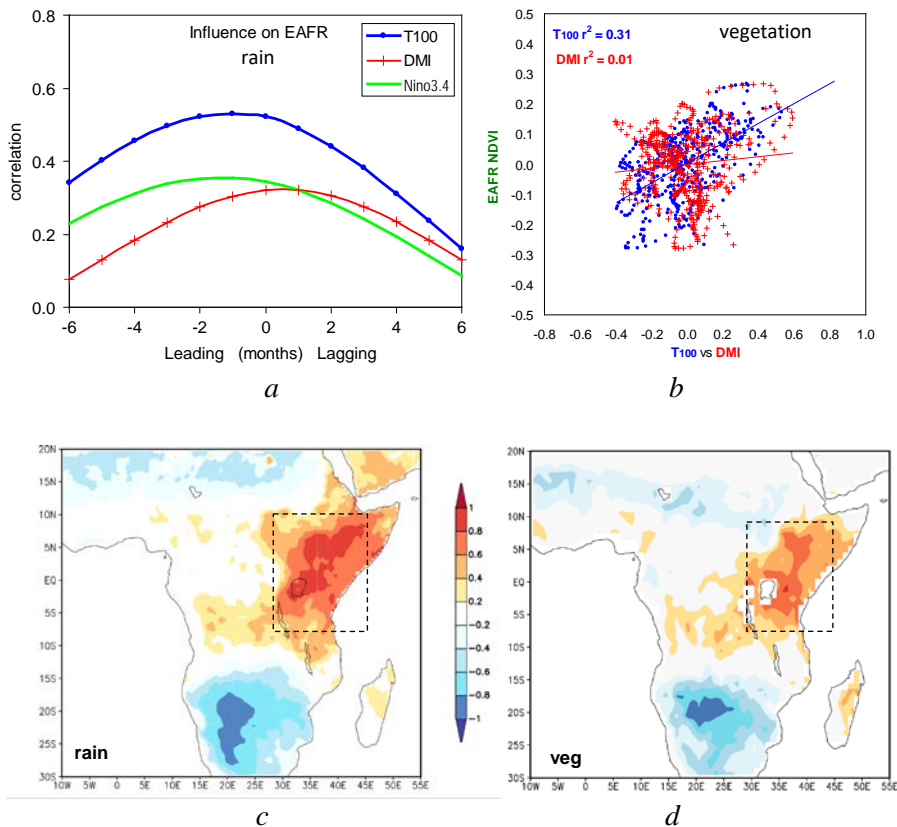
F i g. 7. Lag correlation of East Africa rainfall with T100 EOF1, DMI and Nino3.4 time series from −6 to +6 months (*a*); scatterplot of T100 EOF1 and DMI time series compared with filtered East African NDVI lagged+1 month (*b*); loading patterns for rainfall (*c*) and vegetation that determine the East African cluster (dashed box) used to formulate eafr rain and NDVI time series (*d*)

Summary

Many in the scientific community understand the IOD as an equatorial surface phenomenon involving Bjerknes feedback. This concept may apply elsewhere, but the off-equatorial coupling that drives the Indian Ocean Dipole requires a new perspective. Our research demonstrates that a subsurface off-equatorial index better represents IOD modulation by atmospheric-coupled ocean Rossby waves. Such an index has been derived from the leading EOF mode of standard 1–100 m depth-averaged sea temperatures filtered to retain periods > 1.5 years. The statistical

analysis compared sub-surface and surface Indian Ocean indices (T100, SSH, DMI) with ENSO SST and winds (Nino3.4, −Usfc) and atmospheric convective responses (OLR, eafr). While the DMI [43] uses zonal gradients of SST, the sub-surface temperature dipole in the domain 20°S–5°N, 35°–120°E fully captures the IOD signal and amplified SSH variance on the Seychelles dome ~ 8°S. Zonal oscillations of ocean heat content, quantified by the T100 index, have a steady signal-to-noise ratio (cf. Table 1, Fig. 6, *a*) that typifies resonant fluctuations of the thermocline, less influenced by surface fluxes (cf. Fig. 4, *b*).
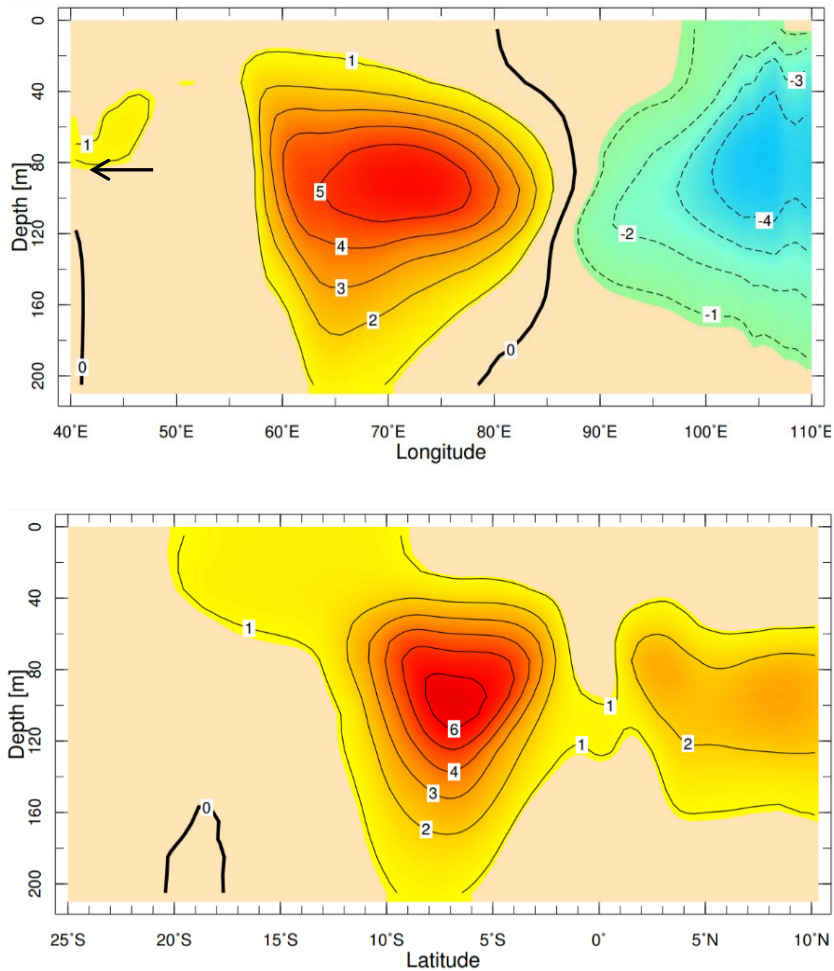
F i g. 8. GODAS September – December 2019 sea temperature anomaly depth sections: longitudinal 5–10ºS (*top*); latitudinal 67–72ºE (*bottom*). Note the +IOD signal south of the equator in the layer 40–140 m

Several domains, parameters and filters were tested to represent the IOD and its regional ocean-atmosphere coupling. Although the DMI serves to highlight a unique mode of interannual ocean-atmosphere variability, it exhibits unsteady temporal coupling with regional atmospheric dipole modes and Pacific ENSO (cf. Fig. 6, *b*), regardless of method employed. A sub-surface index – based on standard

available datasets – offers a more stable representation of the south Indian Ocean Rossby wave [16, 51] that induces climate responses around the basin. A simple EOF analysis of interannual filtered ocean heat content (T100 or SSH), extracts the required signal from fixed centers of action. Consistent with [28], an analysis of the September – December 2019 +IOD (Fig. 8) illustrates a +6 ºC anomaly at 7ºS, 70ºE, 90 m depth which declines to zero in the surface layer from 5ºS–10ºN. We have demonstrated, in side-by-side comparisons of DMI and T100, some benefits of the new index and its linkages [52]. In real-time forecast applications, data-assimilation and coupled model projections offer updated EOF scores for operational use. We view this as a natural progression to better track the amplitude and phase of the Indian Ocean Dipole.

Data availability

A spreadsheet to guide reformulating the IOD index is available from the author on request.

REFERENCES

1. Masumoto, Y. and Meyers, G., 1998. Forced Rossby Waves in the Southern Tropical Indian Ocean. *Journal of Geophysical Research: Oceans*, 103(C12), pp. 27589-27602. doi:10.1029/98JC02546

2. Klein, S.A., Soden, B.J. and Lau N., 1999. Remote Sea Surface Temperature Variations During ENSO: Evidence for a Tropical Atmospheric Bridge. *Journal of Climate*, 12(4), pp. 917-932. doi:10.1175/1520-0442(1999)012<0917:RSSTVD>2.0.CO;2

3. Reppin, J., Schott, F.A., Fischer, J. and Quadfasel, D., 1999. Equatorial Currents and Transports in the Upper Central Indian Ocean: Annual Cycle and Interannual Variability. *Journal of Geophysical Research: Oceans*, 104(C7), pp. 15495-15514. doi:10.1029/1999JC900093

4. Saji, N.H., Goswami, B.N., Vinayachandran, P.N. and Yamagata, T., 1999. A Dipole Mode in the Tropical Indian Ocean. *Nature*, 401, pp. 360-363. doi:10.1038/43854

5. Webster, P.J., Moore, A.M., Loschingg, J.P. and Leben, R.R., 1999. Coupled Ocean-Atmosphere Dynamics in the Indian Ocean During 1997-98. *Nature*, 401, pp. 356-360. doi:10.1038/43848

6. Sengupta, D., Senan, R. and Goswami, B.N., 2001. Origin of Intraseasonal Variability of Circulation in the Tropical Central Indian Ocean. *Geophysical Research Letters*, 28(7), pp. 1267-1270. doi:10.1029/2000GL012251

7. Rao, S.A., Behera, S.K., Masumoto, Y. and Yamagata, T., 2002. Interannual Subsurface Variability in the Tropical Indian Ocean with a Special Emphasis on the Indian Ocean Dipole. *Deep-Sea Research Part II: Topical Studies in Oceanography*, 49(7–8), pp. 1549-1572. https://doi.org/10.1016/S0967-0645(01)00158-8

8. Behera, S.K., Luo, J.J., Masson, S., Rao, S.A., Sakuma, H. and Yamagata, T., 2006. A CGCM Study on the Interaction between IOD and ENSO. *Journal of Climate*, 19(9), pp. 1688-1705. doi:10.1175/JCLI3797.1

9. Yeshanew, A. and Jury, M.R., 2007. North African Climate Variability. Part 1: Tropical Thermocline Coupling. *Theoretical and Applied Climatology,* 89(1–2), pp. 25-36. doi:10.1007/S00704-006-0242-8

10. Izumo, T., Vialard, J., Lengaigne, M., de Boyer Montégut, C., Behera, S.K., Luo, J.-J., Cravatte, S., Masson, S. and Yamagata, T., 2010. Influence of the State of the Indian Ocean Dipole on the Following Year's El Niño. *Nature Geoscience*, 3, pp. 168-172. doi:10.1038/NGEO760

11. Luo, J., Zhang, R., Behera, S.K., Masumoto, Y., Jin, F., Lukas, R. and Yamagata, T., 2010. Interaction between El Niño and Extreme Indian Ocean Dipole. *Journal of Climate*, 23(3),

pp. 726-742. doi:10.1175/2009JCLI3104.1

12. Halkides, D. and Lee, T., 2011. Mechanisms Controlling Seasonal Mixed Layer Temperature and Salinity in the Southwestern Tropical Indian Ocean. *Dynamics of Atmospheres and Oceans*, 51(3), pp. 77-93. doi:10.1016/J.DYNATMOCE.2011.03.002

13. Yokoi, T., Tozuka, T. and Yamagata, T., 2012. Seasonal and Interannual Variations of the SST above the Seychelles Dome. *Journal of Climate*, 25(2), pp. 800-814. doi:10.1175/JCLI-D-10-05001.1

14. Chambers, D.P., Tapley, B.D. and Stewart, R.H., 1999. Anomalous Warming in the Indian Ocean Coincident with El Niño. *Journal of Geophysical Research: Oceans*, 104(C2), pp. 3035-3047. doi:10.1029/1998JC900085

15. Murtugudde, R. and Busalacchi, A.J., 1999. Interannual Variability of the Dynamics and Thermodynamics of the Tropical Indian Ocean. *Journal of Climate*, 12(8), pp. 2300-2326. doi:10.1175/1520-0442(1999)012<2300:IVOTDA>2.0.CO;2

16. White, W.B., 2000. Coupled Rossby Waves in the Indian Ocean on Interannual Timescales. *Journal of Physical Oceanography*, 30(11), pp. 2972-2988. doi:10.1175/1520-0485(2001)031<2972:CRWITI>2.0.CO;2

17. Trenary, L.L. and Han, W., 2012. Intraseasonal-to-Interannual Variability of South Indian Ocean Sea Level and Thermocline: Remote versus Local Forcing. *Journal of Physical Oceanography*, 42(4), pp. 602-627. doi:10.1175/JPO-D-11-084.1

18. Tozuka, T., Nagura, M. and Yamagata, T., 2014. Influence of the Reflected Rossby Waves on the Western Arabian Sea Upwelling Region. *Journal of Physical Oceanography*, 44(5), pp. 1424-1438. https://doi.org/10.1175/JPO-D-13-0127.1

19. Jury, M.R., 2018. South Indian Ocean Rossby Waves. *Atmosphere-Ocean*, 56(5), pp. 322-331. doi:10.1080/07055900.2018.1544882

20. McCreary Jr., J.P., Kundu, P.K. and Molinari, R.L., 1993. A Numerical Investigation of Dynamics, Thermodynamics and Mixed-Layer Processes in the Indian Ocean. *Progress in Oceanography*, 31(3), pp. 181-244. doi:10.1016/0079-6611(93)90002-U

21. Xie, S., Annamalai, H., Schott, F.A. and McCreary Jr., J.P., 2002. Structure and Mechanisms of South Indian Ocean Climate Variability. *Journal of Climate*, 15(8), pp. 864-878. doi:10.1175/1520-0442(2002)015<0864:SAMOSI>2.0.CO;2

22. Huang, B. and Kinter III, J.L., 2002. Interannual Variability in the Tropical Indian Ocean. *Journal of Geophysical Research: Oceans*, 107(C11), 3199. doi:10.1029/2001JC001278

23. Yamagata, T., Behera, S.K., Luo, J-J., Masson, S., Jury, M.R. and Rao, S.A., 2003. Coupled Ocean-Atmosphere Variability in the Tropical Indian Ocean. In: C. Wang, S. Xie and J. Carton, eds., 2003. *Earth's Climate: The Ocean-Atmosphere Interaction*. Geophysical Monograph Series, 147. Washington, DC: AGU, pp. 189-212. doi:10.1029/147GM12

24. Jury, M.R. and Huang, B., 2004. The Rossby Wave as a Key Mechanism of Indian Ocean Climate Variability. *Deep-Sea Research Part I: Oceanographic Research Papers*, 51(12), pp. 2123-2136. doi:10.1016/J.DSR.2004.06.005

25. Wolfe, C.L., Cessi, P. and Cornuelle, B.D., 2017. An Intrinsic Mode of Interannual Variability in the Indian Ocean. *Journal of Physical Oceanography*, 47(3), pp. 701-719. doi:10.1175/JPO-D-16-0177.1

26. Jury, M.R., 2019. Global Wave-2 Structure of El Niño–Southern Oscillation-Modulated Convection. *International Journal of Climatology*, 39(4), pp. 2438-2448. doi:10.1002/joc.5963

27. Nagura, M. and McPhaden, M.J., 2010. Dynamics of Zonal Current Variations Associated with the Indian Ocean Dipole. *Journal of Geophysical Research: Oceans*, 115(C11), C11026. doi:10.1029/2010JC006423

28. Shinoda, T, Hendon, H.H. and Alexander, M.A., 2004. Surface and Subsurface Dipole Variability in the Indian Ocean and Its Relation with ENSO. *Deep-Sea Research Part I:*

Oceanographic Research Papers, 51(5), pp. 619-635. doi:10.1016/J.DSR.2004.01.005

29. Chakravorty, S., Gnanaseelan, C., Chowdary, J.S. and Luo, J.-J., 2014. Relative Role of El Niño and IOD Forcing on the Southern Tropical Indian Ocean Rossby Waves. *Journal of Geophysical Research: Oceans*, 119(8), pp. 5105-5122. https://doi.org/10.1002/2013JC009713

30. Sayantani, O. and Gnanaseelan, C., 2015. Tropical Indian Ocean Subsurface Temperature Variability and the Forcing Mechanisms. *Climate Dynamics*, 44(9–10), pp. 2447-2462. https://doi.org/10.1007/s00382-014-2379-y

31. Deepa, J.S., Gnanaseelan, C., Kakatkar, R., Parekh, A. and Chowdary, J.S., 2018. The Interannual Sea Level Variability in the Indian Ocean as Simulated by an Ocean General Circulation Model. *International Journal of Climatology*, 38(3), pp. 1132-1144. doi:10.1002/joc.5228

32. Levitus, S., Antonov, J.I., Boyer, T.P., Baranova, O.K., Garcia, H.E., Locarnini, R.A., Mishonov, A.V., Reagan, J.R., Seidov, D., Yarosh, E.S. and Zweng, M.M., 2012. World Ocean Heat Content and Thermosteric Sea Level Change (0–2000 m) 1955–2010. *Geophysical Research Letters*, 39(10), L10603. doi:10.1029/2012GL051106

33. Behringer, D.W., 2007. The Global Ocean Data Assimilation System At NCEP. In: AMS, 2007. *11th Symposium on Integrated Observing and Assimilation Systems for the Atmosphere, Oceans, and Land Surface (IOAS-AOLS)*. January 2007, San Antonio, TX, 3.3. Available at: https://ams.confex.com/ams/87ANNUAL/webprogram/Paper119541.html [Accessed: 18 June 2022].

34. Carton, J.A., Chepurin, G.A. and Chen, L., 2018. SODA-3: A New Ocean Climate Reanalysis. *Journal of Climate*, 31(17), pp. 6967-6983. doi:10.1175/JCLI-D-18-0149.1

35. Legeais, J.-F., Ablain, M., Zawadzki, L., Zuo, H., Johannessen, J.A., Scharffenberg, M.G., Fenoglio-Marc, L., Fernandes, M.J., Andersen, O.B. [et al.], 2018. An Improved and Homogeneous Altimeter Sea Level Record from the ESA Climate Change Initiative. *Earth System Science Data*, 10(1), pp. 281-301. doi:10.5194/ESSD-10-281-2018

36. Hersbach, H., Bell, B., Berrisford, P., Hirahara, S., Horanyi, A., Munoz-Sabater, J., Nicolas, J., Peubey, C., Radu, R. [et al.], 2020. The ERA5 Global Reanalysis. *Quarterly Journal of the Royal Meteorological Society*, 146(730), pp. 1999-2049. doi:10.1002/qj.3803

37. Lee, H-T., 2014. *Outgoing Longwave Radiation – Daily - Climate Algorithm Theoretical Basis Document.* NOAA's Climate Data Record Program CDRP-ATBD-0526. NOAA, 46 p. Available at http://www.ncdc.noaa.gov/cdr/operationalcdrs.html [Accessed: 18 June 2022].

38. Funk, C., Peterson, P., Landsfeld, M., Pedreros, D., Verdin, J., Shukla, S., Husak, G., Rowland, J., Harrison, L., [et. al.], 2015. The Climate Hazards Infrared Precipitation with Stations – A New Environmental Record for Monitoring Extremes. *Scientific Data*, 2(1), 150066. doi:10.1038/sdata.2015.66

39. Pinzon, J.E. and Tucker, C.J., 2014. A Non-Stationary 1981-2012 AVHRR NDVI$_3$g Time Series. *Remote Sensing*, 6(8), pp. 6929-6960. doi:10.3390/rs6086929

40. Cleveland, W.S. and Devlin, S.J., 1988. Locally Weighted Regression: An Approach to Regression Analysis by Local Fitting. *Journal of the American Statistical Association*, 83(403), pp. 596-610. doi:10.1080/01621459.1988.10478639

41. Kakatkar, R., Gnanaseelan, C. and Chowdary, J.S., 2020. Asymmetry in the Tropical Indian Ocean Subsurface Temperature Variability. *Dynamics of Atmospheres and Oceans,* 90, 101142. doi:10.1016/j.dynatmoce.2020.101142

42. Roxy, M.K., Gnanaseelan, C., Parekh, A., Chowdary, J.S., Singh, S., Modi, A., Kakatkar, A., Mohapatra, S., Dhara, C., Shenoi, S.C. and Rajeevan, M., 2020. Indian Ocean Warming. In: R. Krishnan, J. Sanjay, C. Gnanaseelan, M. Mujumdar, A. Kulkarni, S. Chakraborty, eds., 2020. *Assessment of Climate Change over the Indian Region*. Singapore: Springer, pp. 191-206. doi:10.1007/978-981-15-4327-2_10

43. Saji, N.H., Xie, S.-P. and Yamagata, T., 2006. Tropical Indian Ocean Variability in the IPCC Twentieth-Century Climate Simulations. *Journal of Climate*, 19(17), pp. 4397-4417.

doi:10.1175/JCLI3847.1

44. Torrence, C. and Compo, G.P., 1998. A Practical Guide to Wavelet Analysis. *Bulletin of American Meteorological Society*, 79(1), pp. 61-78. doi:10.1175/1520-0477(1998)079<0061:APGTWA>2.0.CO;2

45. Bretherton, C.S., Widmann, M., Dymnikov, V.P., Wallace, J.M. and Blade, I., 1999. The Effective Number of Spatial Degrees of Freedom of a Time-Varying Field. *Journal of Climate*, 12(7), pp. 1990-2009. doi:10.1175/1520-0442(1999)012<1990:TENOSD>2.0.CO;2

46. Dima, M. and Lohmann, G., 2004. Fundamental and Derived Modes of Climate Variability: Concept and Application to Interannual Time-Scales. *Tellus A: Dynamic Meteorology and Oceanography*, 56(3), pp. 229-249. doi:10.1111/J.1600-0870.2004.00059.X

47. Blau, M.T. and Ha, K-J., 2020. The Indian Ocean Dipole and Its Impact on East African Short Rains in Two CMIP5 Historical Scenarios with and without Anthropogenic Influence. *Journal of Geophysical Research: Atmospheres*, 125(16), e2020JD033121. doi:10.1029/2020jd033121

48. Fischer, A.S., Terray, P., Guilyardi, E., Gualdi, S. and Delécluse, P., 2005. Two Independent Triggers for the Indian Ocean Dipole/Zonal Mode in a Coupled GCM. *Journal of Climate*, 18(17), pp. 3428-3449. doi:10.1175/JCLI3478.1

49. Behera, S.K., Luo, J., Masson, S., Delecluse, P., Gualdi, S., Navarra, A. and Yamagata, T., 2005. Paramount Impact of the Indian Ocean Dipole on the East African Short Rains: A CGCM Study. *Journal of Climate*, 18(21), pp. 4514-4530. doi:10.1175/JCLI3541.1

50. Nicholson, S.E., 2015. Long-Term Variability of the East African 'Short Rains' and Its Links to Large-Scale Factors. *International Journal of Climatology*, 35(13), pp. 3979-3990. doi:10.1002/joc.4259

51. McIntosh, P.C. and Hendon, H.H., 2018. Understanding Rossby Wave Trains Forced by the Indian Ocean Dipole. *Climate Dynamics*, 50(7–8), pp. 2783-2798. doi:10.1007/s00382-017-3771-1

52. Bracco, A., Kucharski, F., Molteni, F., Hazeleger, W. and Severijns, C., 2005. Internal and Forced Modes of Variability in the Indian Ocean. *Geophysical Research Letters*, 32(12), L12707. doi:10.1029/2005GL023154

53. Reynolds, R.W., Smith, T.M., Liu, C., Chelton, D.B., Casey, K.S. and Schlax, M.G., 2007. Daily High-Resolution Blended Analyses for Sea Surface Temperature. *Journal of Climate*, 20(22), pp. 5473-5496. doi:10.1175/2007JCLI1824.1

54. Rao, S.A. and Behera, S.K., 2005. Subsurface Influence on SST in the Tropical Indian Ocean: Structure and Interannual Variability. *Dynamics of Atmospheres and Oceans*, 39(1–2), pp. 103-135. doi:10.1016/J.DYNATMOCE.2004.10.014

55. Tozuka, T., Yokoi, T. and Yamagata, T., 2010. A Modeling Study of Interannual Variations of the Seychelles Dome. *Journal of Geophysical Research: Oceans*, 115(C4), C04005. doi:10.1029/2009JC005547

About the author:

Mark R. Jury is a professor of meteorology at the University of Puerto Rico Mayaguez and a research fellow of the University of Zululand, South Africa. He holds a PhD from University of Cape Town in 1984, and received the WMO award for best research in 2008, **ORCID ID: 0000-0002-6871-403X**, mark.jury@upr.edu, https://academic.uprm.edu/accam/mark/

The author has read and approved the final manuscript.
The author declares that he has no conflict of interest.